INTERNATIONAL JOURNAL of RENEWABLE ENERGY RESEARCH
M. Srikanth and Y. V. P. Kumar, Vol.16, No.1, March, 2026

PSO Based Modified Pole-Zero Cancellation Technique for VSI Control to Improve Transient Response in Microgrids

M. Srikanth[*], Y. V. Pavan Kumar[**‡]

[*]Department of Electrical and Electronics Engineering, Raghu Engineering College, Visakhapatnam, Andhra Pradesh, INDIA.

[**]School of Electronics Engineering, VIT-AP University, Amaravati 522237, Andhra Pradesh, INDIA.

(srikanth.mandarapu@raghuenggcollege.in, pavankumar.yv@vitap.ac.in)

[‡]Corresponding Author; Y. V. Pavan Kumar, VIT-AP University, Amaravati 522237, Andhra Pradesh, INDIA, Tel: +91863-2370155, pavankumar.yv@vitap.ac.in

Received: 13.01.2024 Accepted:16.02.2024

Abstract - The response of voltage source inverter (VSI) based renewable energy microgrids depends on the control methodology deployed for VSI's power, voltage, and current controllers. Usually, power controllers with fixed droop possess limited power handling capability, which has been addressed by developing adaptive droop control strategies in the literature. However, the efficacy of the adaptive droop control in enhancing the power handling capability depends on the performance of the voltage and current (VA) controllers. However, the VA controllers tuned with conventional PI tuning techniques (PIVA) offer complexity in selecting precise controller gains, which leads to poor transient response. To reduce complexity, the pole-zero cancellation technique (PZC) has been introduced in the literature for VA controllers' tuning. However, the PZC leads to poor transient response during disturbances. Thus, to achieve a better transient response, this paper proposes the design of VA controllers with modified PZC (MPZCVA). This uses particle swarm optimization to optimally tune the integral coefficient based on the error that is observed in the closed loop response against various disturbances. To verify the proposed technique, simulation studies are performed under various power factor loading. Along with the conventional PIVA and proposed MPZCVA controllers, this paper implements fuzzy logic-based adaptive droop (FAD) control for the power controller to form the VSI control loop. Thus, the proposed MPZCVA cascaded with FAD controller (MPZCVA-FAD) is compared with the conventional PIVA cascaded with FAD controller (PIVA-FAD). The results proved the usefulness of the proposed methodology in enhancing the power handling capability and transient response of the microgrid.

Keywords Microgrids, particle swarm optimization (PSO), pole-zero cancellation (PZC), transient response, voltage and current (VA) controllers, voltage source inverter (VSI) control.

Abbreviations

CC	:	Cohen-Coon tuning method	PIVA	:	PI-based VA controllers
FAD	:	Fuzzy logic-based adaptive droop control	PSO	:	Particle swarm optimization technique
FD	:	Fixed droop control for the power controller	PZC	:	Pole zero cancellation technique
ITAE	:	Integral time absolute error	VA	:	Voltage and current controllers
MPZC	:	Modified pole-zero cancellation technique	VSI	:	Voltage source inverter
N	:	Fuzzy membership function named negative	Z	:	Fuzzy membership function named zero
P	:	Fuzzy membership function named positive			

1. Introduction

The rapid growth in consumer demands, depletion of fossil fuel resources, and mounting environmental concerns have driven the pursuit of new and alternative power generation methods [1-3]. Consequently, renewable energy-integrated microgrids emerged as a prospective solution. These microgrids allow for localized power generation at the point of consumption, easing the burden on the main utility grid [4, 5]. However, renewable energy-based microgrids face limitations arising from using static power electronics-based voltage source inverters (VSI) in microgrids. Therefore, it is vital to implement reliable and effective control methodologies that address the critical issues of elevating the transient response of microgrids [6].

The cascaded power-voltage-current controller scheme is a practical and popular control strategy. It is based on multiloop control with the current controller in the innermost loop, the voltage controller in the middle, and the power controller in the outermost loop. Since the voltage-current controllers belong to the inner loop, their operation is much quicker than that of the power loop [7]. A common configuration of the microgrid regulated by a cascaded power-voltage-current control arrangement is shown in Fig.1. In this cascaded power-voltage-current control scheme, the power-handling capability is mainly determined by the power controller. Droop control is commonly used for power controllers, which provides the reference input signal to the voltage and current controllers [8, 9]. Fixed droop (FD) and variable/adaptive droop control are the two types of available droop control strategies. Among the two types, FD controllers have a lower power handling capability than adaptive droop controllers.

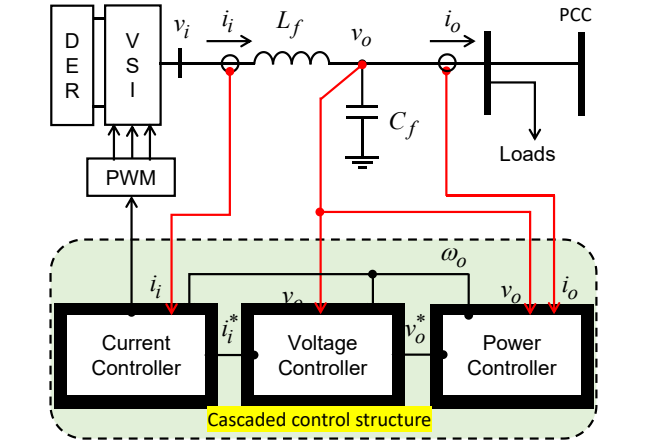

Fig. 1. Microgrid configuration controlled by power voltage and current control scheme.

Therefore, the literature provides insights into different adaptive droop control techniques to improve the microgrid's stability. Adaptive droop control techniques are further classified as offline [10, 11] and online tuning techniques [12-14]. Among these two, online tuning techniques gained popularity because of the minimum dependency on the system's mathematical model. Some state-of-the-art methods under the online category are based on fuzzy logic [12], neural networks [13], and state machine [14]. These conventional adaptive droop-based schemes offer improved stability of the system. However, the effect of voltage-current controllers on the power handling capability of adaptive droop-based control schemes is not fully explored. Thus, for improved transient response of the adaptive droop control-based system, there is a need for a suitable approach to be adopted for the controllers of current and voltage loops.

The controllers for current and voltage loops of the conventional cascaded power-voltage-current control scheme are normally designed in the synchronous reference frame. However, this poses limitations in effectively handling unbalanced disturbances. There are two approaches to improving the performance of voltage-current controllers namely, (i) modern structures for voltage-current controllers [15-18] and (ii) effective tuning techniques for voltage-current controllers [19-24]. This paper attempts performance improvement from the voltage-current controllers' side from the second approach. Literature explored several tuning approaches for voltage-current controllers, such as conventional tuning techniques [19-21], standard tuning approaches based on desired damping factor [22], and pole-zero cancellation (PZC) technique [23, 24]. Of these, PZC implementation is more straightforward. Moreover, PZC tuning greatly reduces the overlap of voltage and current controllers during operation.

The conventional PZC discussed in [23] has not included the power controller in its study. It is verified that the conventional PZC in its original form fails to handle load disturbances when integrated with droop control for the power controller. Therefore, to receive help from PZC-tuned voltage and current controllers when integrated with the droop controller, the modified PZC (MPZC) is presented in this paper. In the proposed MPZC method, the proportional and integral coefficients of the current controller are tuned with the conventional PZC method. However, in the case of the voltage controller, the proportional coefficient is fixed using PZC while the integral coefficient is tuned using the particle swarm optimization (PSO) algorithm. Several works have discussed the use of the PSO algorithm for tuning PI controllers [25-27]. However, one drawback of this algorithm is that the obtained values for the proportional and integral coefficients may not always be feasible. Achieving the desired values often requires more and more iterations. In this work, since the proportional constant is fixed based on PZC, the likelihood of the integral coefficient deviating from the feasible value is significantly reduced. Consequently, the number of iterations needed to bring the integral coefficient value within a feasible range is reduced. Therefore, the proposed MPZC tuning method integrates the strengths of both the PSO algorithm and the PZC method of tuning, resulting in an effective tuning approach. Hereafter, the voltage and current controllers tuned with the proposed MPZC and those with conventional PI tuning techniques are referred to as MPZCVA and PIVA respectively.

The proposed MPZC technique can overcome the limitations of the conventional PI tuning techniques and the recent PZC technique. Thus, to validate the efficacy of the proposed MPZC in enhancing the power handling capability

and transient response of the microgrid, a methodology comprised of MPZCVA and fuzzy logic-based adaptive droop (FAD) is formulated. The response of the proposed methodology (MPZCVA-FAD) is assessed by comparing it with those of conventional methodologies namely, (i) PIVA cascaded with FD controller (PIVA-FD), (ii) MPZCVA cascaded with FD controller (MPZCVA-FD), and (iii) PIVA cascaded with FAD controller (PIVA-FAD).

The other parts of the paper are arranged as follows. The details of the conventional control system is given in section 2. Section 3 discusses PZC implementation for voltage and current controllers and their limitations in the original form. Section 4 presents the implementation of the proposed MPZC and the rationale for its merits over conventional methods. Section 5 analyses the simulation results. Finally, the key achievements of the paper are concluded in section 6.

2. Microgrid Conventional Control System Description

This section describes the conventional designs of power, voltage, and current controllers. Here, section 2.1 describes FD and FAD control schemes for power controllers and section 2.2 describes synchronous reference frame-based voltage-current controllers whose PI controllers are tuned using traditional transient response-based methods.

2.1. FD Control Scheme

The power controller shown in Fig.1 comprises an active and reactive power droop controller. The gains of these controllers are $k_{p\omega}$ and k_{qv}, respectively, and these values are calculated as shown in Eq. (1).

$$\left.\begin{aligned} k_{p\omega} &= \frac{\omega_{o\max} - \omega_{o\min}}{P^*} \\ k_{qv} &= \frac{v_{o\max} - v_{o\min}}{Q^*} \end{aligned}\right\} \quad (1)$$

Output angular frequency ω_o has its maximum and minimum values designated as $\omega_{o\max}$ and $\omega_{o\min}$, while output voltage's v_o maximum and minimum amplitudes are represented by $v_{o\max}$ and $v_{o\min}$, respectively. In the case of a fixed droop scheme, $k_{p\omega}$ and k_{qv} are held fixed throughout the microgrid operation. For a given reference active power P^* and reference angular frequency ω^* the relation between ω_o and P_o is given by Eq. (2). Similarly, for a given reference reactive power Q^* and reference output voltage v_o^*, the relation between v_o and Q_o is given by Eq. (3).

$$\omega_o = \omega^* - k_{p\omega}\left(P_o - P_o^*\right) \quad (2)$$

$$v_o = v_o^* - k_{qv}\left(Q_o - Q_o^*\right) \quad (3)$$

This method efficiently mimics the conventional synchronous behaviour under steady-state conditions but cannot effectively handle transient disturbances.

2.2. FAD Control Scheme

To handle transient stability problems pertaining to frequency and voltage, an adaptive droop control scheme is presented to address the drawbacks of fixed droop control. In the case of fuzzy logic-based control for adaptive droop gain adjustment, the key advantages are flexible nonlinear mapping of inputs with outputs, the robustness with which it handles uncertainties, minimal dependency on the knowledge of the mathematical model, linguistic interpretability for human-readable representation of the control system and its adaptability to changes in system dynamics. Fuzzy logic control is used to adjust the droop coefficients $k_{p\omega}$ and k_{qv}. In this procedure, only half of these droop coefficients i.e., A_P and A_Q are adjusted with fuzzy logic and the other half F_P and F_Q are held fixed. The corresponding equations which denote this procedure are shown in Eq. (4) and the corresponding schematic diagram is shown in Fig.2. The rules of the fuzzy inference system and the ranges fixed to each of the variables used in the inference system are portrayed in Fig. 3.

$$\left.\begin{aligned} k_{p\omega} &= F_P + A_P \\ k_{qv} &= F_Q + A_Q \\ F_P &= 0.5k_{p\omega} \text{ and } F_Q = 0.5k_{qv} \end{aligned}\right\} \quad (4)$$

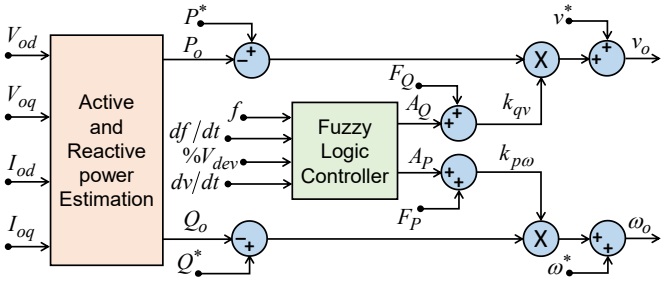

Fig. 2. Schematic diagram of FAD control scheme.

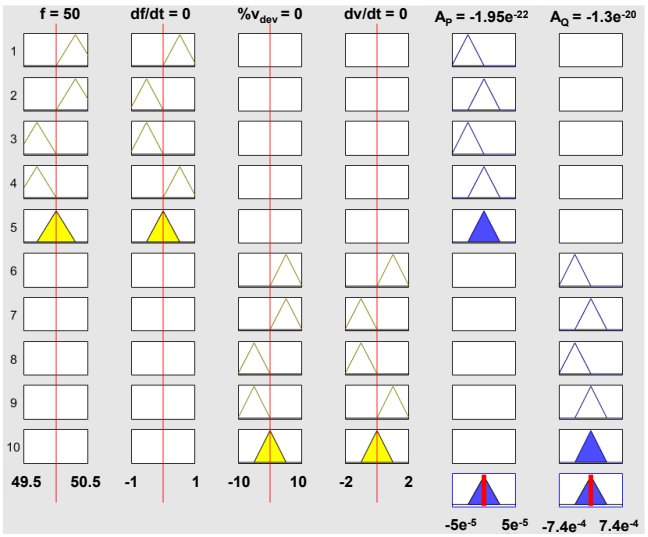

Fig. 3. Rules of FAD's fuzzy inference system.

As depicted in Fig.2, the fuzzy controller receives four inputs and provides two outputs. The two outputs are A_P and A_Q, and the four inputs are output frequency (*f*), output frequency gradient (*df/dt*), deviation percentage in output voltage *(%vdev)*, and output voltage gradient (*dv/dt*). The

fuzzy inference system maps the outputs with the inputs. Each of the four input variables and two output variables is assigned three triangle membership functions as shown in in Fig. 3. They are represented as negative (N), zero (Z), and positive (P). Inputs *f* and *df/dt* determine the output A_P; *%vdev* and *dv/dt* determine the output A_Q. Further, the details about these fuzzy rules are available in [28].

2.3. Conventionally Tuned Voltage and Current Controllers

The layout showing voltage and current control modules designed in a synchronous reference frame is shown in Fig.4. These modules' performance relies on the tuning of the PI controllers, as seen in the forward paths of these controllers.

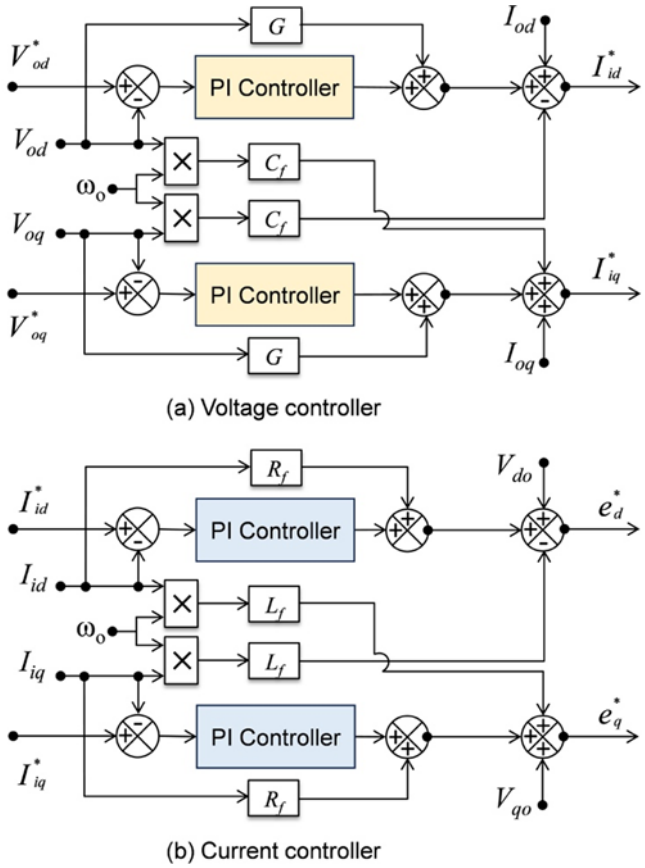

(a) Voltage controller

(b) Current controller

Fig. 4. Schematic of voltage and current controllers.

Several tuning techniques are available in the literature. They are mainly classified into two categories: error performance index-based and open loop transient response-based. It is proved in [23] that the CC method from the open loop transient response category provides the best performance. Thus, this paper uses the CC tuning method as the conventional tuning technique for tuning PI controllers of voltage/current control loops.

3. PZC-based Tuning of VA Controllers

This section describes the conventional PZC method of tuning the controllers of voltage and current loops. In a cascaded scheme, the voltage controller receives the voltage reference signal from the droop controller. After that, the current signal obtained as output from the voltage controller is fed as a reference input signal to the current controller, which finally, after processing, provides a reference signal to the pulse width modulation.

3.1. Current Controller Tuning

The current control loop is the innermost of all, and it regulates the inverter's output current (i_i) by comparing it with the inverter reference current (i_i^*). With v_i as the inverter terminal voltage and v_o as the output voltage available at the load, the dynamics at the AC side of the VSI in the *dq* reference frame is given by Eq. (5). R_f is the resistance of filter inductance L_f. As seen in Eq. (5), the d and q-axis voltage equations have coupling terms. By introducing control inputs that encapsulate these coupling terms, the decoupling of the d and q axes is achieved [29]. After decoupling, the plant's transfer function is given by Eq. (6).

$$\left.\begin{aligned} v_{id} &= R_f i_{1d} + L_f \frac{di_{1d}}{dt} - \omega_o L_f i_{1q} + v_{od} \\ v_{iq} &= R_f i_{1q} + L_f \frac{di_{1q}}{dt} + \omega_o L_f i_{1d} + v_{oq} \end{aligned}\right\} \quad (5)$$

$$G_{sA}(s) = \frac{1}{sL_f + R_f} \quad (6)$$

When a PI controller $K_A(s)$ shown in Eq. (7) is used to regulate i_i with respect to i_i^*, the corresponding schematic diagram of the current control loop is shown in Fig.5. Its open-loop transfer function is given in Eq. (8). If the tunings are made to the PI-current controller's proportional and integral gains as shown in Eq. (9), the open-loop transfer function will transform to Eq. (10). Thus, the closed-loop transfer function of the current loop is given in Eq. (11).

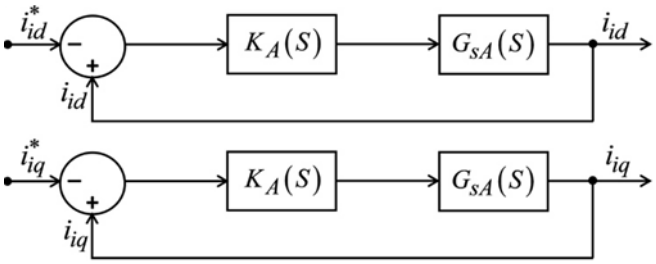

Fig. 5. Model of the VSI's current control loop.

$$K_A(s) = \frac{K_{IA} + sK_{PA}}{s} \quad (7)$$

$$\left.\frac{i_{id}(s)}{i_{id}^*}\right|_{OL} = \left.\frac{i_{iq}(s)}{i_{iq}^*}\right|_{OL} = K_A(s) * G_{sA}(s) \quad (8)$$

$$\frac{K_{IA}}{K_{PA}} = \frac{R_f}{L_f} \quad (9)$$

$$\left.\frac{i_{id}(s)}{i_{id}^*}\right|_{OL} = \left.\frac{i_{iq}(s)}{i_{iq}^*}\right|_{OL} = \frac{K_{PA}}{sL_f} \quad (10)$$

$$\left.\frac{i_{id}(s)}{i_{id}^*}\right|_{CL} = \left.\frac{i_{iq}(s)}{i_{iq}^*}\right|_{CL} = \frac{1}{1+s\tau_1}; where\ \tau_1 = \frac{L_f}{K_{PA}} \quad (11)$$

3.2. *Voltage Controller Tuning*

The voltage loop adjusts the output voltage v_o by comparing it with v_o^*. Since load current primarily dictates v_o, the dynamic equations in *dq* form, which represent the dynamics of the load, are shown in Eq. (12).

$$\left.\begin{aligned} C_f \frac{dv_{od}}{dt} &= \omega_o C_f v_{oq} + i_{1d} - i_{od} \\ C_f \frac{dv_{oq}}{dt} &= -\omega_o C_f v_{od} + i_{1q} - i_{oq} \end{aligned}\right\} \tag{12}$$

C_f is the filter capacitance. As seen in Eq. (12), the d and q-axis equations are coupled. By introducing control inputs that encapsulate these coupling terms, the d and q axes become decoupled [30]. The transfer function of the plant after decoupling is given by Eq. (13). The tuning of the voltage loop follows the design of the current control loop. Thus, when a PI controller $K_V(s)$ shown in Eq. (14) is introduced to regulate v_o with respect to v_o^*, the closed loop transfer function of the current controller should also be included. The corresponding block diagram of the voltage control loop is shown in Fig.6, and Eq. (15) shows the corresponding open-loop transfer function.

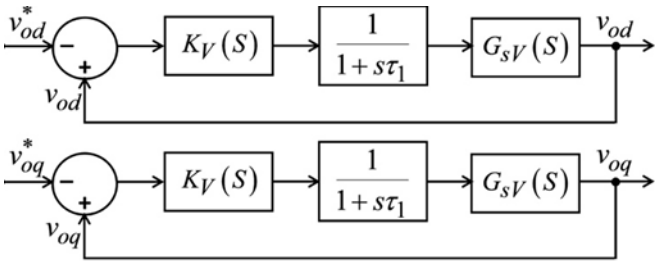

Fig. 6. Block diagram of the voltage control loop.

$$G_{sV}(s) = 1/sC_f \tag{13}$$

$$K_V(s) = (K_{IV} + sK_{PV})/s \tag{14}$$

$$\left.\frac{v_{od}(s)}{v_{od}^*}\right|_{OL} = \left.\frac{v_{oq}(s)}{v_{oq}^*}\right|_{OL} = \frac{K_{IV} + sK_{PV}}{s^2 C_f} \tag{15}$$

By assigning $K_{IV} = 0$, the voltage controller's closed-loop transfer function is given as Eq. (16). If the adjustments are made to the PI-voltage controller's proportional and integral gains as shown in Eq. (16), the open-loop transfer function becomes Eq. (17).

$$\left.\frac{v_{od}(s)}{v_{od}^*}\right|_{OL} = \left.\frac{v_{oq}(s)}{v_{oq}^*}\right|_{OL} = \frac{K_{PV}}{sC_f} \tag{16}$$

$$\left.\frac{v_{od}(s)}{v_{od}^*}\right|_{CL} = \left.\frac{v_{oq}(s)}{v_{oq}^*}\right|_{CL} = \frac{1}{1+s\tau_2} \tag{17}$$

where, $\tau_2 = \dfrac{C_f}{K_{PV}}$

4. Proposed MPZC Technique

This section explains the execution of the proposed methodology, with reference to the schematic presented in Fig.7. The proposed methodology uses fuzzy logic for adaptive droop coefficient adjustment, and the modified pole-zero cancellation technique (MPZC) is used to tune the PI controllers of the voltage and current control loops. The details of fuzzy logic-based adaptive droop adjustment techniques are discussed in section 2.2. In this section, the implementation of MPZC for tuning voltage and current controllers is discussed.

4.1. *Rationale of the Proposed MPZC Method of Tuning*

The performance of current controllers tuned with the PZC method is satisfactory. While tuning the voltage controllers with the PZC method, it is assumed to consider K_{IV} as zero. Theoretically, the analysis is correct, and the performance is satisfactory when the d and q axes are completely decoupled. However, the complete decoupling between the d and q axis is not maintained in case of a disturbance. Moreover, while designing the voltage controllers, the transfer function of the current controller based on the decoupling principle is included. This further aggravates the problem. To mitigate the disadvantage of the conventional PZC tuning method, while retaining the advantage of the same, the value of K_{PV} is fixed at the same value as obtained by the conventional PZC method. However, K_{IV} is adjusted to a non-zero value by using PSO.

4.2. *Objective Function and Problem Formulation*

The PI controller of the voltage loop compares the output voltage with the voltage reference and produces a control signal to minimize the error *e(t)*. The output of the PI controller is expressed as shown in Eq. (18).

$$u(t) = K_{PV} * e(t) + K_{IV} \int e(t) \tag{18}$$

Zero steady state voltage difference is attained by reducing the integral time absolute error (ITAE) of the objective function given by Eq. (19). Finally, the optimization problem is framed as shown in Eq. (20). The constraint ensures that the value of the decision variable 'K_{IV}' is limited within the feasible region represented as $x_{lowerbound}$ and $x_{upperbound}$ respectively.

$$F = t \times \int_0^{t_{sim}} \left| v_i^* - v_i \right| dt \tag{19}$$

$$\left.\begin{aligned} &Minimize\ F(x) \\ &x = K_{IV} \\ &subject\ to\ x_{lowerbound} \le x \le x_{upperbound} \end{aligned}\right\} \tag{20}$$

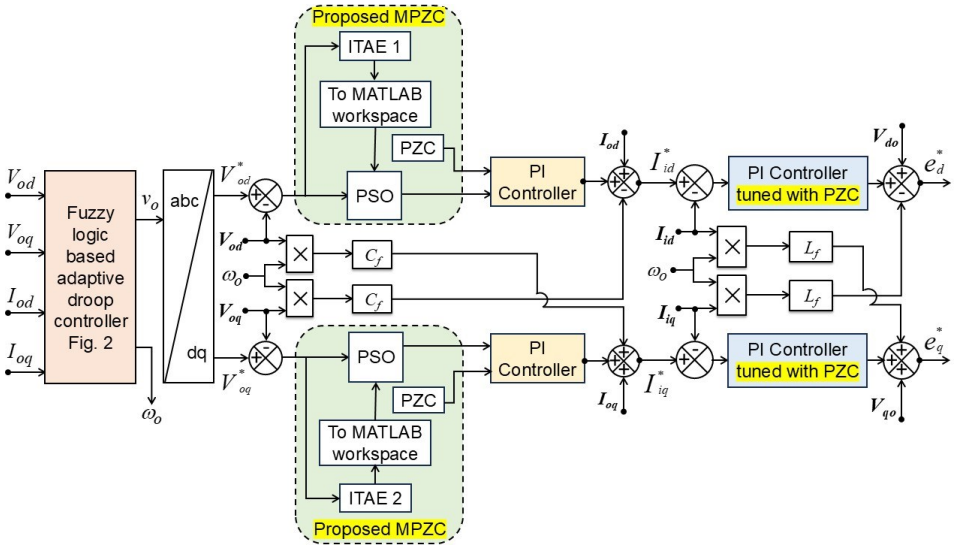

Fig. 7. Block diagram of the proposed VSI's control methodology.

4.3. PSO Method of Solving the Problem

PSO stands as a metaheuristic optimization algorithm, employing a population of particles traversing a search space to discover the best solution for a given problem. Each particle denotes a potential solution, dynamically adjusting its position by drawing upon its individual experience and the shared knowledge of the entire swarm. Through iterative updates of particle velocity and position, influenced by both individual and global best positions, PSO effectively traverses the search space, gradually converging toward the optimal solution. It begins with initializing the population of the 'n' number of particles in the search space and initializing the number of decision variables 'm'. Each particle has a position vector $X_i = [x_{i,1}, x_{i,2}, ..., x_{i,n}]^T$ representing a potential solution and each particle also has a velocity vector $V_i = [v_{i1}, v_{i2}, ..., v_{in}]^T$ indicating the direction and speed of movement. In general, the vector of the i^{th} particle in the population is defined as X_i^t shown in Eq. (21) for iteration t, where i=1, 2…, n and m=1, 2…, j. For the present case, there is only one decision variable K_{IV}, therefore the vector X_i^t is expressed as shown in Eq. (22).

$$X_i^t = \left[X_{i,1}^t, X_{i,2}^t, X_{i,3}^t, ...X_{i,m}^t \right] \quad (21)$$

$$X_i^t = \left[X_{i,1}^t \right] = \left[K_{IVi}^t \right] \quad (22)$$

In the next stage, the fitness of each particle $F\left(K_{IVi}\right)$ is assessed depending on the problem's objective function wherein the fitness value indicates the position quality of the particle. The existing fitness value of the i^{th} particle is evaluated in relation to its best fitness value $P_{Best,i}$, it has previously reached. In case the existing fitness is greater than $P_{Best,i}$, then update $P_{Best,i}$ and remember the corresponding position $X_{Best,i}$. Later, the updated fitness of each particle is checked against the best fitness value reached by any particle up to the present moment, G_{Best}. In case the present fitness is better than G_{Best}, update G_{Best} and remember the corresponding position X_{Best}. In the next stage, the velocity and position of each particle are updated using the equation shown in Eq. (23) and Eq. (24) respectively. Here, 'w' is the inertia weight that dictates the influence of the particle's prior velocity, while c_1 and c_2 are acceleration coefficients denoting the cognitive and social components, r_1 and r_2 are random numbers between 0 and 1.

$$V_i(t+1) = c_1 r_1 (P_{Best,i} - X_i) + w V_i(t) + c_2 r_2 (G_{Best,i} - X_i) \quad (23)$$

$$X_i^t = \left[X_{i,1}^t \right] = \left[K_{IVi}^t \right] \quad (24)$$

The procedure repeats until a termination criterion namely, the maximum count of iterations (t_{max}) is arrived and the desired fitness value is achieved. The final position vector of the particle with the best fitness value (G_{Best}) represents the optimal K_{IV} value for the given problem. The pseudo-code of the PSO algorithm used for the proposed method is displayed in Table 1.

Table 1. PSO algorithm used for the proposed method

Pseudo Code:
Start
Initialize the population 'n' and decision variable 'K_{IV}' within the search space
Initialize V_i and X_i for each particle
Set P_{Best} and G_{Best} in the given population
Set feasible region of values for K_{IV}
Set the maximum number of iterations
while $t \leq t_{max}$
for $i = 1: n$
update particle's velocity $V_i(t+1)$ as per (23)
update particle's position $X_i(t+1)$ as per (24)
evaluate the fitness $P_{Best,i}$ of particle's new position
end for
for $i = 1: n$
if fitness of the new position is better than the particle's best fitness
update particle's best fitness and position

end if
if fitness of the new position is better than the global best fitness
update global best fitness and position
end if
end for
end while
return G_{Best} as optimal solution of decision variable 'K_{IV}'
end

5. Simulation and Discussion

The test microgrid of this study comprises one DG unit with a rated capacity of 25kW+j25kVar and two three-phase loads (load-1 and load-2). An LC filter connects the DG unit to the load, which receives power from the source when the corresponding breaker gets closed. The system model is implemented in MATLAB/Simulink software. The input DC voltage of VSI is 540V and the filter parameters are R_f = 0.1mohm, L_f=1mH, and C_f=5mf. The control specifications of the system are shown in Table 2.

Table 2. Voltage and current controller's coefficients.

Coefficient	Description	CC	PZC	MPZC
K_{PA}	Proportional coefficient of the current controller	3.2 $\times 10^{-3}$	1.2 $\times 10^{-1}$	1.2 $\times 10^{-1}$
K_{IA}	Integral coefficient of the current controller	1 $\times 10^{-1}$	6.7	6.7
K_{PV}	Proportional coefficient of voltage controller	4 $\times 10^{-3}$	5.65 $\times 10^{-4}$	5.65 $\times 10^{-4}$
K_{IV}	Integral coefficient of voltage controller	3.02 $\times 10^{-5}$	0	2.48 $\times 10^{-1}$

The study system is simulated with four different control methodologies, and the performance of these systems is evaluated under five test cases (T1-T5). While load-1 is a fixed type that exists throughout the operation, load-2 is a variable load that remains active between 80-90sec. Therefore between 80-90secs, the net load seen by the system is the sum of load-1 and load-2. Hence, load-2 is selected carefully, so the resultant load during 80-90sec will destabilize one of the conventional methodologies. This is the principle in setting different test cases, whose details are presented in Table 3.

Table 3. Summary of different test cases

Test case	Load-1 (kW+jkVar)	Load-2 (kW+jkVar)	Power factor		
			0-80 sec	80-90 sec	90-160 sec
T1	1.2+j0.3	0.3+j0.5	0.97	0.88	0.97
T2	1.2+j0.3	0.3+j1.0	0.97	0.76	0.97
T3	1.2+j0.3	0.3+j1.5	0.97	0.64	0.97
T4	1.2+j0.3	0.3+j2.5	0.97	0.47	0.97
T5	1.2+j0.3	0.3+j3.5	0.97	0.37	0.97

The four control methodologies tested in this work are i) conventional PIVA-FD, ii) conventional MPZCVA-FD, iii) conventional PIVA-FAD, and iv) proposed MPZCVA-FAD. The testing of these methodologies is taken up in two phases to ensure clarity of results. Initially, conventional PIVA-FD and MPZCVA-FD schemes are tested under T1-T3. Later, conventional PIVA-FAD and proposed MPZCVA-FAD schemes are tested under T3-T5.

5.1. Test Cases T1and T2

As mentioned earlier in this section, conventional PIVA-FD and MPZCVA-FD are tested during these test cases. The corresponding frequency and voltage results with the PIVA-FD method are seen in Fig.8 and Fig.9, respectively. Similarly, the frequency and voltage results with the MPZCVA-FD method under these test cases are seen in Fig.10 and Fig.11, respectively. Frequency results seen in Fig.8(a) and Fig.10(a) confirm the ability of both methods to maintain stability. This identification is further confirmed by the voltage results, as shown in Fig.8(a) and Fig.10(a), which show no waveform distortions. During T2, as Fig.8(b) noticed, the frequency output with the PIVA-FD method has exceeded the permissible limits. This shows that the PIVA-FD method has failed to maintain stability. This stability loss is confirmed by distorted voltage results shown in Fig.9(b).

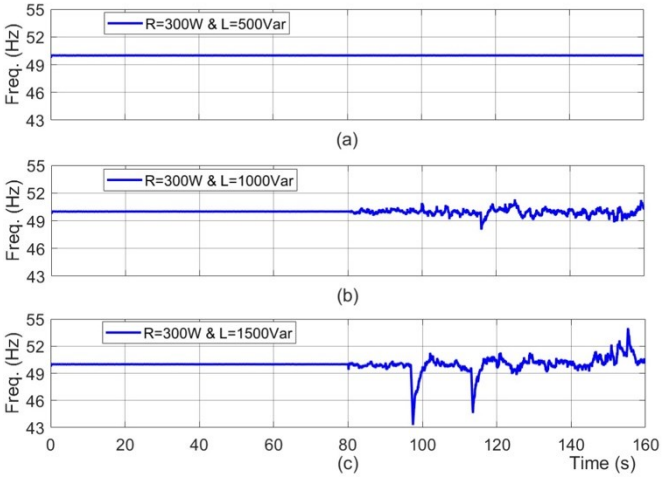

Fig. 8. Frequency response with conventional PIVA-FD method under (a) T1, (b) T2, and (c) T3.

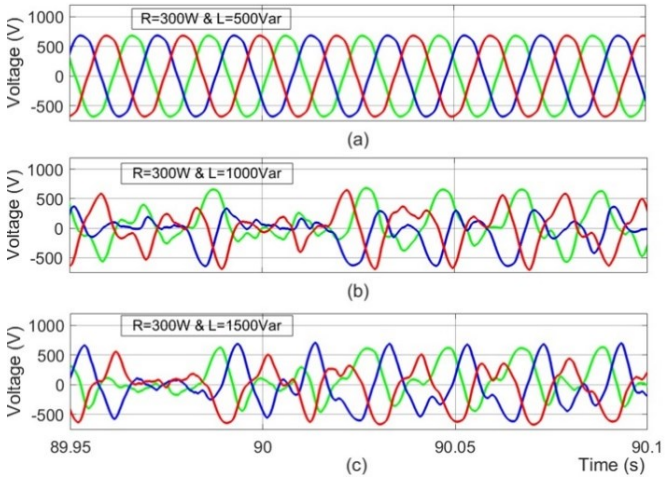

Fig. 9. Voltage response with conventional PIVA-FD under (a) T1, (b) T2, and (c) T3.

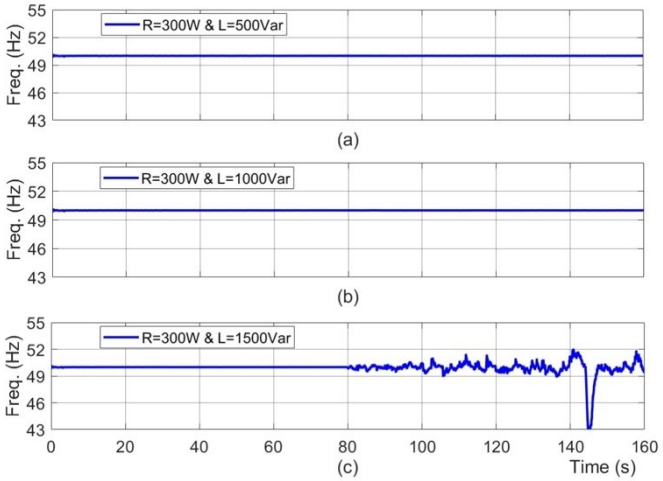

Fig. 10. Frequency response with conventional MPZCVA-FD method under (a) T1, (b) T2, and (c) T3.

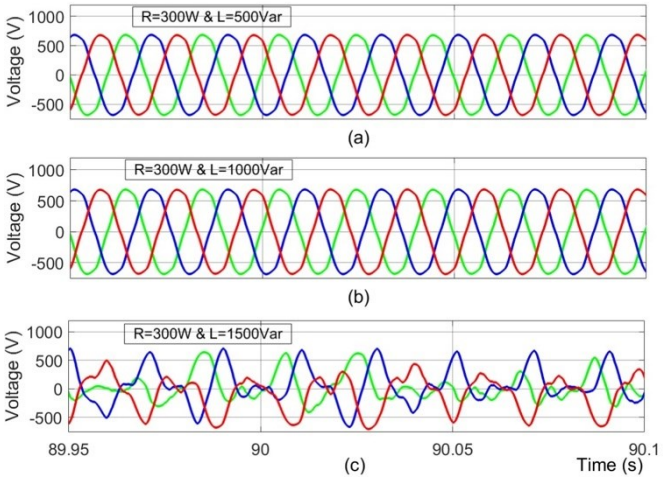

Fig. 11. Voltage response with conventional MPZCVA-FD method under (a) T1, (b) T2, and (c) T3.

The frequency stability limits are 51Hz on the upper side and 49Hz on the lower side. This criterion is used to verify frequency stability in all the test cases. In contrast, during T2, the MPZCVA-FD method had maintained stability. The confirmation of this is seen in Fig.10(b) and Fig.11(b). This confirms that the proposed MPZC method can enhance the power handling capability of the power controller.

5.2. Test Case T3

During T3, the MPZCVA-FD method failed to maintain stability. The frequency result from Fig.10(c) and voltage result from Fig.11(c) confirms the inability. The frequency results with PIVA-FAD and the proposed MPZCVA-FAD show that both methods can maintain stability. This confirms the need to replace the fixed droop logic with adaptive droop logic to enhance the power handling capability. The frequency result of both methods is very much within the stability band, as seen in Fig.12. Furthermore, the voltage results shown in Fig.13 show no distortions. However, superior performance from the proposed MPZCVA-FAD method than the conventional PIVA-FD method can be observed from the active power and reactive power output results, as shown in Fig.14 and Fig.15, respectively. The key identifications that justify the supremacy of the proposed MPZCVA-FAD methodology above the conventional PIVA-FAD methodology from test case T3 are mentioned as follows.

- During startup, the proposed methodology reached a steady state faster than the conventional methodology which took around 40 sec to settle.
- At 80 sec, concerning overshoot in active power, as seen in Fig.14, the proposed methodology has produced less overshoot than the conventional methodology.
- As seen from Fig.14 and Fig.15, even though load-2 is disconnected at 90 seconds, a prolonged operation is seen with the conventional methodology. However, the proposed methodology shows an immediate change after 90 seconds, which is very desirable for good transient response.
- The undershoot in active power after disconnection of load-2 with the proposed methodology is much lesser than with the conventional methodology.
- The overshoot in reactive power after disconnection of load-2 with the proposed methodology is almost nil when compared to the conventional methodology.

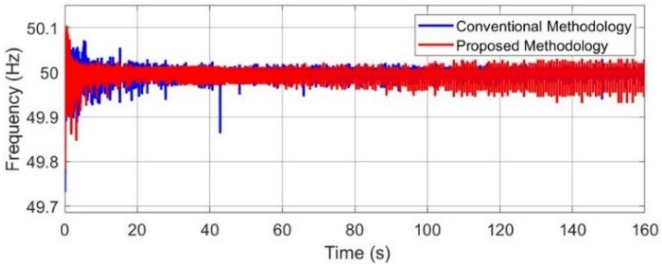

Fig. 12. Frequency response of conventional PIVA-FAD and proposed MPZCVA-FAD during T3.

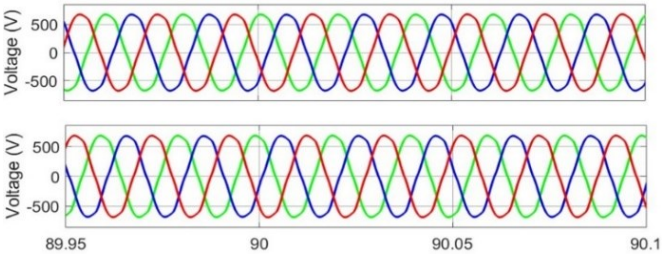

Fig. 13. Voltage during T3 with conventional PIVA-FAD (upper trace) and proposed MPZCVA-FAD (lower trace).

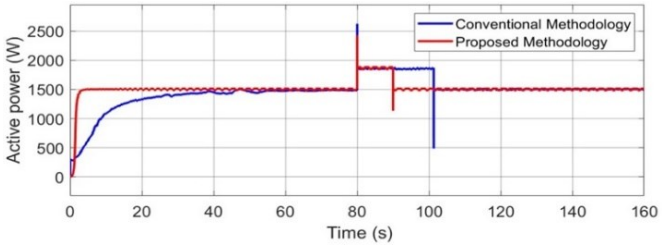

Fig. 14. Active power responses of conventional PIVA-FAD and proposed MPZCVA-FAD during T3.

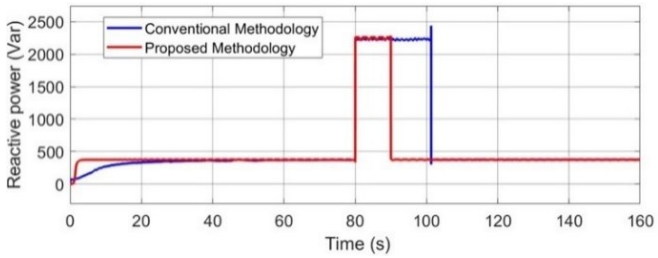

Fig. 15. Reactive power responses of conventional PIVA-FAD and proposed MPZCVA-FAD during T3.

5.3. Test Case T4

During T4, the responses of the conventional PIVA-FD method and the proposed MPZCVA-FAD method are shown in Fig.16 to Fig.19. From the frequency result shown in Fig.16, both methods have successfully maintained frequency stability. However, after disconnection of load-2, i.e., around 90sec, a little distortion is seen in the frequency result with the conventional method. Since this deviation is slight, no impact is seen in the voltage output as shown in Fig.17. But, the impact of this distortion in frequency result is seen in the active/reactive power output results, as shown in Fig.18 and Fig.19. The key identifications noted in T3 are valid in this test case also.

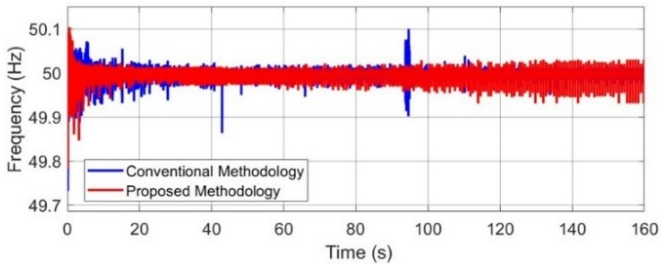

Fig. 16. Frequency response of conventional PIVA-FAD and proposed MPZCVA-FAD during T4.

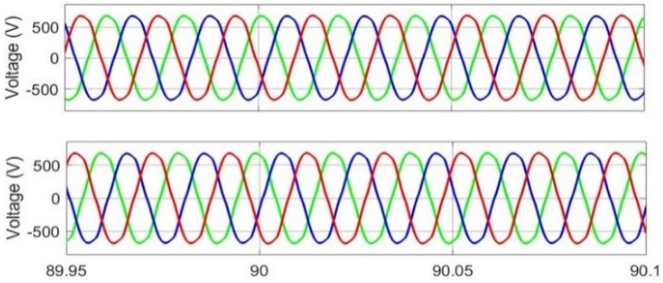

Fig. 17. Voltage during T4 with conventional PIVA-FAD (upper trace) and proposed MPZCVA-FAD (lower trace).

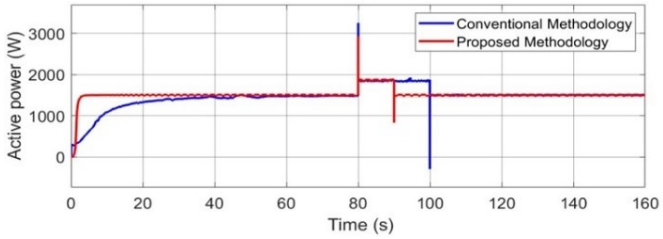

Fig. 18. Active power responses of conventional PIVA-FAD and proposed MPZCVA-FAD during T4.

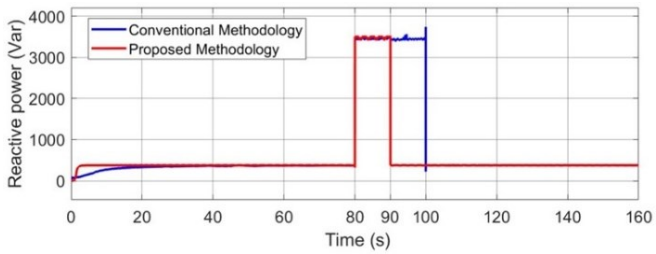

Fig. 19. Reactive power responses of conventional PIVA-FAD and proposed MPZCVA-FAD during T4.

5.4. Test Case T5

During T5, the responses of the conventional PIVA-FD method and the proposed MPZCVA-FAD method are shown from Fig.20 to Fig.23. The frequency results shown in Fig.20 demonstrate the failure of the conventional method and the ability of the proposed method to maintain stability. This is further confirmed by the voltage result, as shown in Fig.21, where the voltage output of the conventional PIVA-FD method is heavily distorted while the voltage quality with the proposed method is satisfactory. The active and reactive power output results are shown in Fig.22 and Fig.23, respectively. It is seen from these results that, after disconnection of load-2 at 90sec, the proposed method has continued to perform satisfactorily. In contrast, the conventional method has failed to deliver the required active and reactive powers. This test case confirms that the proposed MPZC method has allowed the voltage and current controllers to extend their support in enhancing the power handling capability of the adaptive droop control.

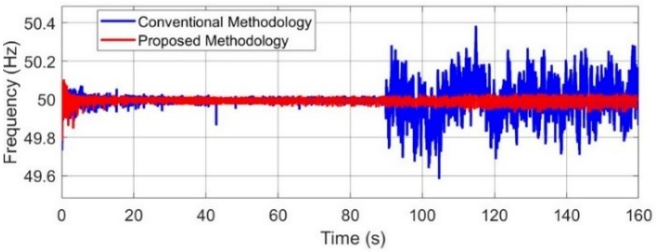

Fig. 20. Frequency response of conventional PIVA-FAD and proposed MPZCVA-FAD during T5.

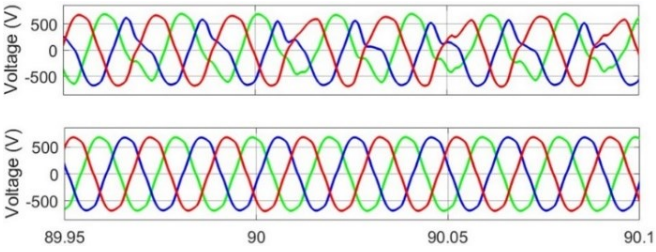

Fig. 21. Voltage during T5 with conventional PIVA-FAD (upper trace) and proposed MPZCVA-FAD (lower trace).

A summary of the test results of different conventional and proposed methodologies under different test cases T1-T5 is presented in Table 4. In this table, NA refers to "not applicable", and "Failed" indicates stability failure.

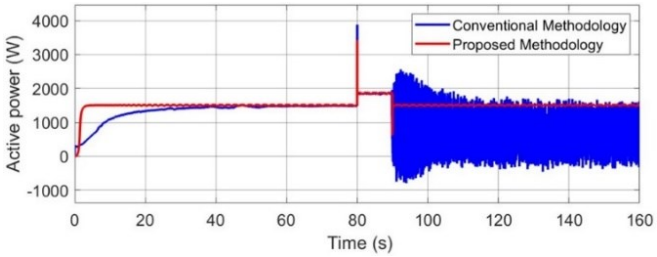

Fig. 22. Active power responses of conventional PIVA-FAD and proposed MPZCVA-FAD during T5.

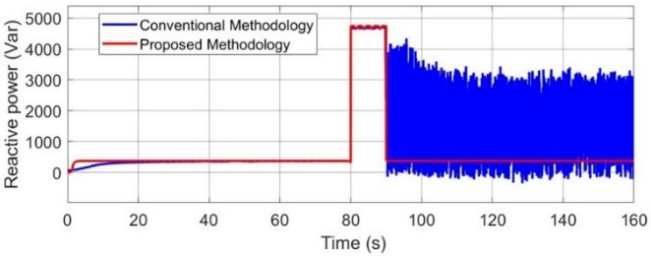

Fig. 23. Reactive power responses of conventional PIVA-FAD and proposed MPZCVA-FAD during T5.

Table 4. Summary of test results obtained with the conventional and proposed methodologies

Characteristics		Test Case	Conv. PIVA-FD (I) [9], [20]	Conv. MPZCVA-FD (II) [23]	Conv. PIVA-FAD (III) [28], [32]	Prop. MPZCVA-FAD (IV)	Best Method
Frequency characteristics Desired Limits: ▪ Max: 51 Hz Min: 49 Hz (IEEE 1547)	Max value (Hz)	T1	50	50	50	50	All
		T2	51.5	50.1	50	50	II, III, IV
		T3	54	52	50	50	III, IV
		T4	56.3	54.7	50.1	50	III, IV
		T5	58.6	56.9	50.4	50	IV
	Min value (Hz)	T1	50	50	50	50	All
		T2	48	50	50	50	II, III, IV
		T3	43	42	50	50	III, IV
		T4	41.8	41.2	49.9	50	III, IV
		T5	40.0	39	49.6	50	IV
Power characteristics Desired: ▪ System stability: Stable ▪ Extra burden: low ▪ Recovery time: less	System stability (Pass / Fail)	T1	Pass	Pass	Pass	Pass	All
		T2	Failed	Pass	Pass	Pass	II, III, IV
		T3	Failed	Failed	Pass	Pass	III, IV
		T4	Failed	Failed	Pass	Pass	III, IV
		T5	Failed	Failed	Failed	Pass	IV
	Extra burden (Watts)	T3	NA	NA	900	600	IV
		T4	NA	NA	1400	1100	IV
		T5	NA	NA	NA	1500	IV
	Load recovery (sec)	T3	NA	NA	10	0	IV
		T4	NA	NA	10	0	IV
		T5	NA	NA	NA	0	IV
Voltage characteristics Desired: ▪ Quality: 200V max for 600V peak (IEEE C62.41.2) ▪ Start-up time: 0 sec	Peak change (volts)	T3	Failed	Failed	85	56	IV
		T4	Failed	Failed	285	64	IV
		T5	Failed	Failed	Failed	73	IV
	Start-up (sec)	T1	16	0	16	0	II, IV
		T2	16	0	16	0	II, IV
		T3	16	0	16	0	II, IV
		T4	16	0	16	0	II, IV
		T5	16	0	16	0	II, IV

6. Conclusion

This paper proposes a modified pole-zero cancellation technique for tuning the controllers of the current and voltage control loops of the microgrid's VSI. This proposed tuning technique uses the PSO algorithm to design the integral coefficient of the voltage controller. The output of the proposed MPZCVA-FAD methodology is compared with three conventional methodologies, namely, PIVA-FD, MPZCVA-FD, and PIVA-FAD, under five test cases T1-T5 as defined in Table 3. Based on the analysis of test results shown in Fig.8 to Fig.23, and from Table 4, the salient identifications of this work are provided as follows.

- In Test Case T2, it is observed that the maximum frequency deviation using the conventional PIVA-FD method was 51.5 Hz, whereas with the conventional MPZCVA-FD method, it is reduced to 50.1 Hz. This signifies the MPZC as an effective tuning technique.
- In all test cases, it is observed that the methodologies with MPZCVA offered a quicker start-up (around 1 sec) than the conventional PIVA (around 16 sec).

- In Test Case T4, it is observed that the conventional PIVA-FAD method resulted in an overshoot of 1400W in active power at the instant of load switch-on. However, the proposed MPZCVA-FAD method led to a lesser overshoot of 1100W under the same conditions. This proves that the proposed method will comparatively reduce overshoot in active power under load switch on.
- During T3 and T4, the conventional PIVA-FAD method took around 10 sec to return to normalcy after the load switched off, while the proposed method quickly returned around 1 sec to normalcy.
- Under T5, the proposed method by maintaining stability has demonstrated that the power handling capability of the adaptive droop scheme can be pushed further with MPZC-tuned voltage and current controllers.

The results validate the superior response of the proposed method (MPZCVA-FAD) against the conventional methodologies (PIVA-FD, MPZCVA-FD, and PIVA-FAD), emphasizing its effectiveness in enhancing the power handling capability and transient response in microgrids.

Acknowledgements

This work was supported by the Project Grant No: VIT-AP/SpoRIC/RGEMS/2023-24/002, sponsored by "Research Grant in Engineering, Management and Science (RGEMS)" scheme of VIT-AP University, Amaravati 522237, Andhra Pradesh, INDIA.

Author Contributions

M.S. was responsible for the conceptualization, validation, resources, data curation, software development, and project administration. M.S. and Y.V.P. jointly contributed to the methodology, formal analysis, investigation, original draft preparation, review and editing, visualization, supervision, and funding acquisition. All authors have read and agreed to the published version of the manuscript.

Conflict of Interest

The author(s) declared no potential conflicts of interest with respect to the research, authorship, and/or publication of this article.

References

[1] A. Mohammed and H. Abu-Rub, "A co-simulation platform for microgrid integration into transmission system—Power quality study," in Proc. 10th Int. Conf. Smart Grid (icSmartGrid), Istanbul, Turkey, 2022, pp. 319–324, doi: 10.1109/icSmartGrid55722.2022.9848679.

[2] I. E. Davidson and E. Buraimoh, "Modeling and fault ride-through control strategy for grid-supporting photovoltaic-based microgrids," Int. J. Smart Grid, vol. 7, no. 2, Jun. 2023, doi: 10.20508/ijsmartgrid.v7i2.284.g273.

[3] M. Abdou-Tankari, J. Arkhangelski, M. Garba, G. Lefebvre, A. Drame, and D. Abdourahimou, "Power quality challenges and urban microgrid based grid resiliency: Case of Niamey city electrical grid," in Proc. 12th Int. Conf. Renewable Energy Research and Applications (ICRERA), Oshawa, ON, Canada, 2023, pp. 79–86, doi: 10.1109/ICRERA59003.2023.10269391.

[4] N. Altin and S. E. Eyimaya, "A review of microgrid control strategies," in Proc. 10th Int. Conf. Renewable Energy Research and Application (ICRERA), Istanbul, Turkey, 2021, pp. 412–417, doi: 10.1109/ICRERA52334.2021.9598699.

[5] A. AlKassem, M. Al Ahmadi, and A. Draou, "Modeling and simulation analysis of a hybrid PV-wind renewable energy sources for a micro-grid application," in Proc. 9th Int. Conf. Smart Grid (icSmartGrid), Setubal, Portugal, 2021, pp. 103–106, doi: 10.1109/icSmartGrid52357.2021.9551215.

[6] M. Srikanth, Y. V. P. Kumar, M. Amir, S. Mishra, and A. Iqbal, "Improvement of transient performance in microgrids: Comprehensive review on approaches and methods for converter control and route of grid stability," IEEE Open J. Ind. Electron. Soc., vol. 4, pp. 534–572, Oct. 2023, doi: 10.1109/OJIES.2023.3325440.

[7] M. Srikanth and Y. V. P. Kumar, "Improved virtual synchronous generator-based control scheme for enhanced transient response in microgrids," Eng. Proc., vol. 56, no. 1, 2023, doi: 10.3390/ASEC2023-15390.

[8] J. Schiffer, R. Ortega, A. Astolfi, J. Raisch, and T. Sezi, "Conditions for stability of droop-controlled inverter-based microgrids," Automatica, vol. 50, pp. 2457–2469, Oct. 2014, doi: 10.1016/j.automatica.2014.08.009.

[9] M. Guan, W. Pan, J. Zhang, Q. Hao, J. Cheng, and X. Zheng, "Synchronous generator emulation control strategy for voltage source converter (VSC) stations," IEEE Trans. Power Syst., vol. 30, no. 6, pp. 3093–3101, Nov. 2015, doi: 10.1109/TPWRS.2014.2384498.

[10] D. K. Dheer, N. Soni, and S. Doolla, "Improvement of small signal stability margin and transient response in inverter-dominated microgrids," Sustain. Energy Grids Netw., vol. 5, pp. 135–147, Mar. 2016, doi: 10.1016/j.segan.2015.12.005.

[11] J. Alipoor, Y. Miura, and T. Ise, "Stability assessment and optimization methods for microgrid with multiple VSG units," IEEE Trans. Smart Grid, vol. 9, no. 2, pp. 1462–1471, Mar. 2018, doi: 10.1109/TSG.2016.2592508.

[12] A. Anilkumar and N. V. Srikanth, "Teaching-learning optimization based adaptive fuzzy logic controller for frequency control in an autonomous microgrid," Int. J. Renewable Energy Res., vol. 7, no. 4, 2017, doi: 10.20508/ijrer.v7i4.6337.g7238.

[13] J. Kaushal and P. Basak, "Power quality control based on voltage sag/swell, unbalancing, frequency, THD and power factor using artificial neural network in PV integrated AC microgrid," Sustain. Energy Grids Netw.,

vol. 23, Art. no. 100365, Sep. 2020, doi: 10.1016/j.segan.2020.100365.

[14] M. Srikanth and Y. V. P. Kumar, "A state machine-based droop control method aided with droop coefficients tuning through infeasible range detection for improved transient performance of microgrids," Symmetry, vol. 15, no. 1, p. 1, 2022, doi: 10.3390/sym15010001.

[15] C. Andalib-Bin-Karim, X. Liang, and H. Zhang, "Fuzzy-secondary-controller-based virtual synchronous generator control scheme for interfacing inverters of renewable distributed generation in microgrids," IEEE Trans. Ind. Appl., vol. 54, no. 2, pp. 1047–1061, Mar. 2018, doi: 10.1109/TIA.2017.2773432.

[16] W. Ma, Y. Guan, and B. Zhang, "Active disturbance rejection control based control strategy for virtual synchronous generators," IEEE Trans. Energy Convers., vol. 35, no. 4, pp. 1747–1761, Dec. 2020, doi: 10.1109/TEC.2020.2991737.

[17] Y. Wang, D. Wang, Z. Huang, and Y. Li, "Hybrid voltage and current control strategy for virtual synchronous generator under unbalanced voltage conditions," IET Renewable Power Generation, 2022, doi: 10.1049/rpg2.12497.

[18] Y. Zhu, H. Wang, and Z. Zhu, "Improved VSG control strategy based on the combined power generation system with hydrogen fuel cells and super capacitors," Energy Rep., vol. 7, pp. 6820–6832, Nov. 2021, doi: 10.1016/j.egyr.2021.10.056.

[19] B. V. Murthy, Y. V. P. Kumar, and U. V. R. Kumari, "Application of neural networks in process control: Automatic/online tuning of PID controller gains for ±10% disturbance rejection," in Proc. IEEE Int. Conf. Adv. Commun. Control Comput. Technol., 2012, pp. 348–352, doi: 10.1109/ICACCCT.2012.6320800.

[20] T. Wen, J. Liu, C. Tongwen, and H. J. Marquez, "Comparison of some well-known PID tuning formulas," Comput. Chem. Eng., vol. 30, no. 9, pp. 1416–1423, 2006, doi: 10.1016/j.compchemeng.2006.04.001.

[21] O. D. Aidan, Handbook of PI and PID Controller Tuning Rules, 3rd ed. London, U.K.: Imperial College Press, 2009.

[22] C. Bajracharya, M. Molinas, J. A. Suul, and T. M. Undeland, "Understanding of tuning techniques of converter controllers for HVDC," in Proc. Nordic Workshop Power Ind. Electron. (NORPIE), Helsinki, Finland, 2008, pp. 1–8.

[23] Y. V. P. Kumar and R. Bhimasingu, "Design of voltage and current controller parameters using small signal model-based pole-zero cancellation method for improved transient response in microgrids," SN Appl. Sci., vol. 3, p. 836, 2021, doi: 10.1007/s42452-021-04815-x.

[24] Đ. M. Stojić and T. B. Šekara, "A new digital resonant current controller for AC power converters based on the advanced Z-transform," ISA Trans., vol. 139, pp. 535–545, Oct. 2022, doi: 10.1016/j.isatra.2022.02.008.

[25] U. Sultana, S. H. Qazi, N. Rasheed, and M. W. Mustafa, "Performance analysis of real-time PSO tuned PI controller for regulating voltage and frequency in an AC microgrid," Int. J. Electr. Comput. Eng., vol. 11, no. 2, pp. 1068–1076, Apr. 2021, doi: 10.11591/ijece.v11i2.pp1068-1076.

[26] G. Štimac, S. Braut, and R. Žigulić, "Comparative analysis of PSO algorithms for PID controller tuning," Chin. J. Mech. Eng., vol. 27, pp. 928–936, Dec. 2014, doi: 10.3901/CJME.2014.0527.302.

[27] S. Behera, B. Subudhi, and B. B. Pati, "Design of PI controller in pitch control of wind turbine: A comparison of PSO and PS algorithm," Int. J. Renewable Energy Res., vol. 6, no. 1, 2016, doi: 10.20508/ijrer.v6i1.3137.g6783.

[28] Y. V. P. Kumar and R. Bhimasingu, "Fuzzy logic based adaptive virtual inertia in droop control operation of the microgrid for improved transient response," in Proc. IEEE PES Asia-Pacific Power and Energy Engineering Conf. (APPEEC), Bangalore, India, 2017, pp. 1–6, doi: 10.1109/APPEEC.2017.8309006.

[29] M. Yazdanian and A. Mehrizi-Sani, "Internal model-based current control of the RL filter-based voltage-sourced converter," IEEE Trans. Energy Convers., vol. 29, no. 4, pp. 873–881, Dec. 2014, doi: 10.1109/TEC.2014.2353035.

[30] M. Yazdanian and A. Mehrizi-Sani, "Case studies on cascade voltage control of islanded microgrids based on the internal model control," IFAC-PapersOnLine, vol. 48, no. 30, pp. 578–582, Dec. 2015, doi: 10.1016/j.ifacol.2015.12.442.

[31] M. Yadav, P. Jaiswal, and N. Singh, "Fuzzy logic-based droop controller for parallel inverter in autonomous microgrid using vectored controlled feed-forward for unequal impedance," J. Inst. Eng. India Ser. B, vol. 102, no. 4, pp. 691–705, 2021, doi: 10.1007/s40031-021-00588-4.